Title
Observational evidence against strongly stabilizing tropical cloud feedbacks

Journal
Geophysical Research Letters, 44(3)

ISSN
0094-8276

Authors
Williams, Ian N
Pierrehumbert, Raymond T

Publication Date
2017-02-16

DOI
10.1002/2016gl072202

Peer reviewed

Observational evidence against strongly stabilizing tropical cloud feedbacks

Ian N. Williams

Raymond T. Pierrehumbert
First published: 19 January 2017
https://doi.org/10.1002/2016GL072202
UC-eLinks

Abstract

We present a method to attribute cloud radiative feedbacks to convective processes, using subcloud layer buoyancy as a diagnostic of stable and deep convective regimes. Applying this approach to tropical remote sensing measurements over years 2000–2016 shows that an inferred negative short-term cloud feedback from deep convection was nearly offset by a positive cloud feedback from stable regimes. The net cloud feedback was within statistical uncertainty of the National Center for Atmospheric Research Community Atmosphere Model (CAM5) with historical forcings, with discrepancies in the partitioning of the cloud feedback into convective regimes. Compensation between high-cloud responses to tropics-wide warming in stable and unstable regimes resulted in smaller net changes in high-cloud fraction with warming. In addition, deep convection and associated high clouds set in at warmer temperatures in response to warming, as a consequence of nearly invariant subcloud buoyancy. This invariance further constrained the magnitude of cloud radiative feedbacks and is consistent with climate model projections.

1 Introduction

Tropical clouds contribute to much of the uncertainty in climate sensitivity to greenhouse gas radiative forcing [*Wetherald and Manabe*, 1988; *Ramanathan et al.*, 1989]. Low-level clouds are the largest source of intermodel variance in climate projections [*Bony and Dufresne*, 2005; *Webb et al.*, 2006; *Soden and Vecchi*, 2011; *Sherwood et al.*, 2014]. However, there remains uncertainty in the radiative effects of deep convection and associated high clouds. It was recently estimated that observed climate sensitivity is near the lower end of the range of climate model predictions and that a modest reduction in the high climate sensitivities of some models could be achieved by adding a model temperature dependence to the precipitation efficiency of deep convection [*Mauritsen and Stevens*, 2015]. A related study found a decrease in tropical high-cloud amount with warming due to clustering or aggregation of deep convection in a climate model [*Bony et al.*, 2016]. On the other hand, efforts to explicitly resolve deep convection at global scale suggest a large positive high-cloud feedback [*Tsushima et al.*, 2014], which may be sensitive to subgrid turbulence and microphysics parameterizations [*Bretherton*, 2015].

Observational estimates of deep convective cloud feedback are challenging in part because deep convection is coupled to large-scale climate dynamics in addition to surface temperature. Past estimates were based on local covariation of cloud radiative effect (CRE) and sea surface temperature (SST) [*Ramanathan and Collins*, 1991; *Lindzen et al.*, 2001] and were confounded by the tendency for deep convection and warm SSTs to coincide with large-scale ascent [*Fu et al.*, 1992; *Wallace*, 1992; *Hartmann and Michelsen*, 1993; *Lau et al.*, 1994, 1997; *Hartmann and Michelsen*, 2002]. Moreover, high-cloud feedback may be governed by different processes in regions of deep convection (and large-scale ascent) compared to remote stable regions, since only half of all tropical cirrus clouds are formed by detrainment from deep convection [*Luo and Rossow*, 2004]. Understanding of deep convective cloud feedback could be improved by separating the intrinsic temperature response of clouds from the influence of large-scale circulation on cloud type and convective regimes. Additionally, a method to control for the influences of large-scale circulation would help eliminate one possible source of the time scale dependence of cloud feedbacks noted previously [*Zhou et al.*, 2016] and thus would aid in evaluating climate predictions against short-term observations.

Here we use a measure of subcloud layer buoyancy (B) to partition the cloud feedback into convective regimes. Deep convection and associated high clouds set in when the subcloud layer is buoyant with respect to the free troposphere ($B > 0$). Moreover, when negative, B is a measure of inversion strength, which is highly correlated with low clouds [*Klein and Hartmann*, 1993; *Wood and Bretherton*, 2006]. Definitions of deep convection based on B are largely invariant under tropics-wide warming, as shown here. A related method based on midtropospheric vertical velocity (ω_{500}) [*Bony et al.*, 2004] is expected to yield similar results for deep convection, since ω_{500} and B are dynamically coupled; i.e., where B is positive, deep convection contributes to large-scale ascent. Therefore, B reflects both the large-scale circulation and the thermodynamic environment to which it is coupled. Unlike ω_{500}, stability-related metrics such as B can better distinguish between shallow and deep clouds [*Medeiros and Stevens*, 2011; *Webb et al.*, 2015]. Furthermore, B can be calculated independently from thermodynamic soundings, whereas ω_{500} must be derived from climate models.

Our objectives are to (1) demonstrate the utility of a buoyancy-based diagnostic of tropical cloud radiative effects, (2) diagnose observed short-term cloud feedbacks from clouds in deep convective and stable regimes, and (3) evaluate cloud feedbacks in a climate model.

2 Diagnosing Cloud Radiative Effects of Deep Convection

We used monthly TOA shortwave and longwave all-sky radiation measured from CERES (Clouds and Earth's Radiant Energy System) on the Terra satellite (CERES EBAF-TOA Ed2.8) *Wielicki et al.* [1996], and SST from the U.S. National Oceanic and Atmospheric Administration (NOAA) optimal interpolation data set [*Reynolds and Smith*, 1994; *Reynolds et al.*, 2002]. CRE was calculated by subtracting the clear-sky from the all-sky radiative fluxes, using clear-sky fluxes from the European Centre for Medium-Range Weather Forecasts (ECMWF) interim reanalysis product at 1° × 1° resolution [*Dee et al.*, 2011], as in *Dessler* [2010] and *Dessler and Loeb* [2013]. The resulting CRE was adjusted to account for noncloud effects using a radiative kernel approach [*Shell et al.*, 2008]. We focused our analysis on the tropical oceans (30°S to 30°N), for years CERES data were available (March 2000 to May 2016). We compared CERES observations to a climate model simulation (1979–2006), from the Atmospheric Model Intercomparison Project (AMIP). We used a single run from the National Center for Atmospheric Research (NCAR) Community Atmosphere Model (CAM5.1) at 1° × 1° resolution with historical forcings (hereafter CAM5-AMIP). Years 1982–1983 and 1991–1992 were excluded due to volcanic aerosol.

To explore the relationship between CRE and SST, we averaged shortwave and longwave CRE within SST intervals of 0.5°C to obtain their SST distributions (Figure 1a). The threshold SST for deep convection is indicated by the sharp rise in shortwave and longwave CRE between 26 and 29°C (Figure 1a). The observed near cancelation between shortwave and longwave CRE [*Kiehl*, 1994] results in a smaller net cooling effect of clouds near the convective threshold SST. Note that CRE drops off at very high SSTs greater than 30°C, which has been interpreted in relation to large-scale circulations [*Waliser*, 1996] and wind evaporation feedback on SST “hot spots” [*Sobel and Gildor*, 2003].

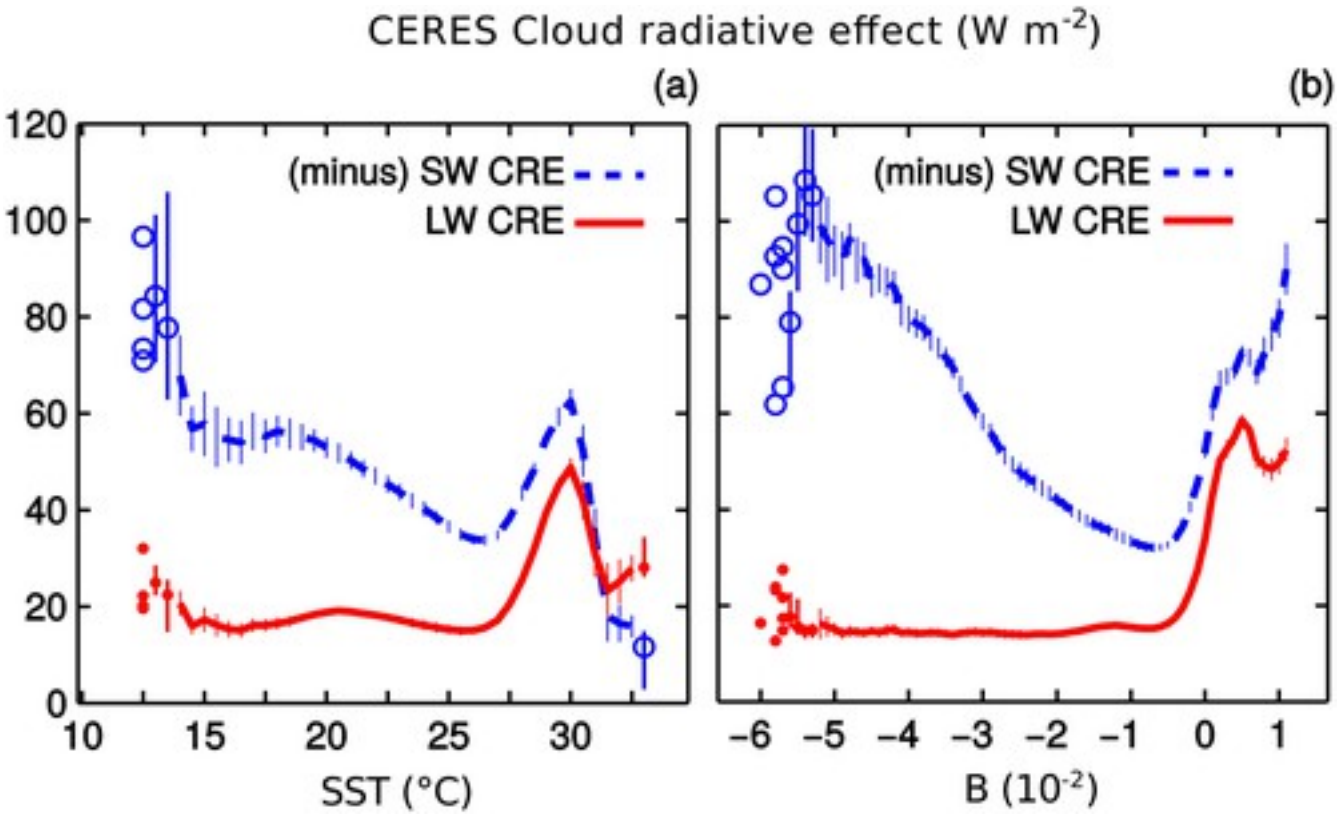

Figure 1

Open in figure viewerPowerPoint

(a) Distribution of monthly cloud radiative effect (CRE) shown as a function of SST and (b) nondimensional subcloud layer buoyancy (i.e., *B*), over tropical oceans. Deep convection is indicated by the sharp increase in both (minus) shortwave (dashed blue lines) and longwave (solid red lines) CRE between 27 and 29°C. CRE declines over the warmest SSTs (SST >30), whereas CRE generally increases with $B > 0$. Error bars indicate the standard error of the mean. Circles with error bars show the interquartile range for bins having less than 20 data points, and circles without error bars show individual data points.

Caption

To diagnose the convective processes influencing cloud type and CRE, we replaced SST with a measure of subcloud buoyancy (*B*). *B* is proportional to the difference between the unsaturated moist static energy of the subcloud layer (h_0), and the saturated moist static energy of the overlying free troposphere (h^*). This follows from the temperature difference between cloudy air and the environment in the tropics. The free-tropospheric temperature profile can be approximated by a saturated moist adiabat, while the cloudy air originates near the surface and conserves moist static energy up to the cloud base [*Randall*, 2015]. This diagnostic is similar to the “entropy excess” introduced earlier [*Williams et al.*, 2009]. However, moist static energy allows an approximate expression for buoyancy at cloud base to be written compactly as

$$B = \frac{h_0 - h^*}{c_p T (1 + \gamma)} \quad (1)$$

where B is the buoyancy nondimensionalized by the gravitational acceleration and c_p is the specific heat of dry air. T represents the temperature at cloud base, which for our purposes can be approximated by the near-surface air temperature (see supporting information S1 for details). Although variations in B are largely controlled by the numerator in equation 1, the denominator gives the expression convenient units of acceleration when B is multiplied by gravitational acceleration. The additional factor $(1 + \gamma)$ arises from the temperature dependence of the saturation mixing ratio,

$$\gamma = \frac{L}{c_p} \frac{\mathrm{d}q^*}{\mathrm{d}T} \quad (2)$$

where L is the latent heat of vaporization and the change in saturation mixing ratio (q^*) with temperature is evaluated at constant pressure.

We calculated B using ECMWF interim reanalysis. Other reanalysis products gave similar results. We averaged h^* over the free troposphere between 300 and 925 hPa, and averaged $h_0$between 925 and 1000 hPa. There was little sensitivity to the exact choice of levels, although differences between modeled and observed B were larger when calculating h_0 using surface values at 2 m. The buoyancy distribution of CRE was calculated by averaging CRE within Bintervals of 10^{-3}. The spatial distributions of stable and unstable regimes are shown in supporting information Figure S1.

Shortwave and longwave CRE sharply increase above $B = 0$ (Figure 1b), indicating the presence of deep convection and high clouds. Cloud radiative effects are more clearly delineated by B, particularly in very stable and unstable regimes. The larger shortwave CRE under stable conditions is characteristic of low clouds and is consistent with previous work showing that low cloud amount is strongly correlated with lower tropospheric inversion strength [*Klein and Hartmann*, 1993] and subsidence [*Bony and Dufresne*, 2005]. Furthermore, the comparison of SST and B coordinates suggests that the hottest SSTs are not actually in areas of strong buoyancy. In fact, they are rather stable or neutrally stable regions (Figure S2). Instead, the maximum cloud radiative effect and maximum buoyancy are both occurring at somewhat cooler temperatures.

3 Response of Cloud Radiative Effect to Warming

We estimated distributions of CRE over SST and B during the 2015–2016 El Niño, and for the three coldest years in the CERES record as determined by averaging annual SSTs over the tropical oceans (30°S to 30°N). The averaging was performed from June to May, to maximize

interannual variability associated with the El Niño–Southern Oscillation. The difference in average SST between the 2015–2016 El Niño year and the coldest years (2000, 2007, and 2011) was 0.60°C. The comparison (Figure 2a) shows that the convective threshold increases with tropics-wide warming, as seen by the shift in onset of strong CRE beyond 26°C.

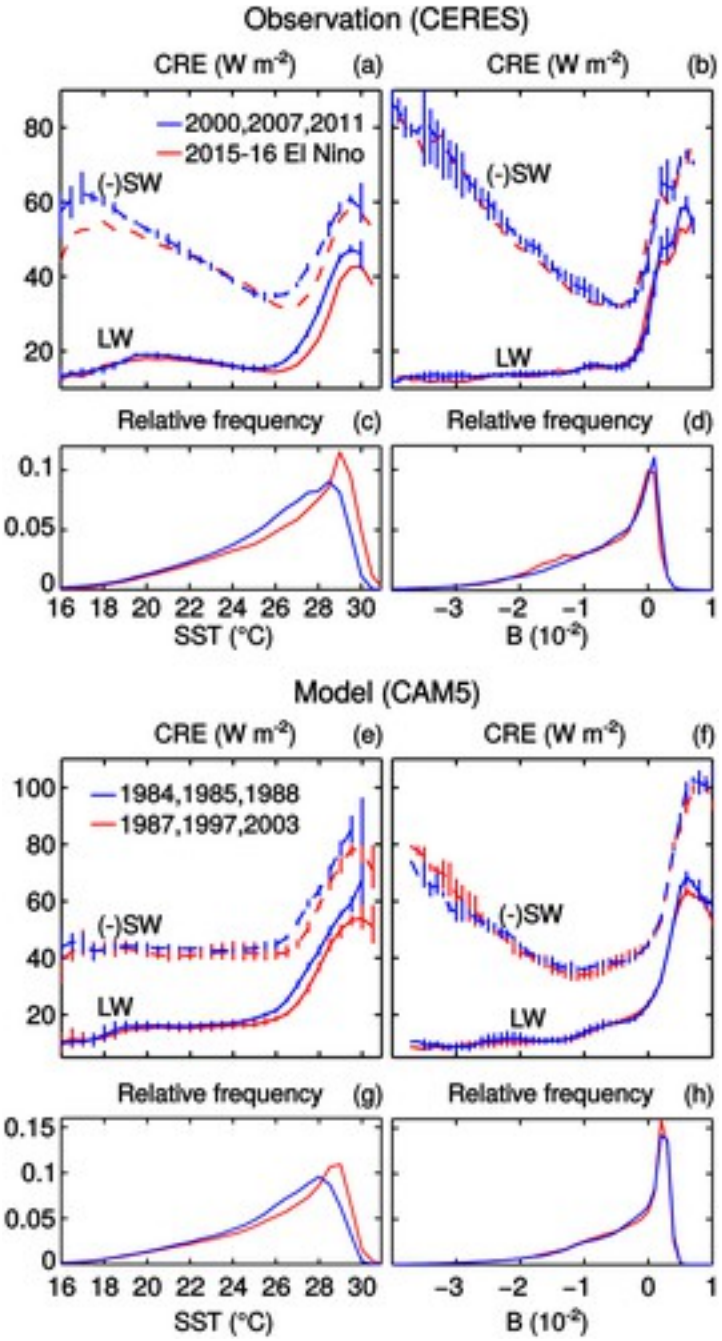

Figure 2

Open in figure viewerPowerPoint

Effects of tropics-wide SST variability on observed and modeled CRE, shown as functions of local SST (Figures 2a, 2c, 2e, and 2g) and *B* (Figures 2b, 2d, 2f, and 2h). (a) The SST

distributions of (minus) shortwave (dashed lines) and longwave (solid lines) CRE shift almost uniformly to warmer SSTs during the 2015–2016 El Niño relative to the three coldest years observed. (b) The buoyancy distribution of CRE is approximately invariant with warming. (c) Relative frequency distributions show that warming is approximately uniform across SST. (d) Warming results in little change to the relative frequency distribution of buoyancy. (e–h) As in Figures 2a–2d but for CAM5-AMIP simulations, for the three warmest and coldest simulated years. Error bars indicate the range over all three years.
Caption

The success of *B* in controlling for variations in the convective threshold is indicated by the approximate collapse of the warmest and coldest years CRE onto a single curve when plotted as a function of *B* (Figure 2b). A similar result was obtained for the Coupled Model Intercomparison Project (CMIP3), for the scenario in which equivalent CO_2 concentration starts at preindustrial levels and increases 1% yr^{-1} until doubling [*Williams et al.*, 2009, Figures 1b and 1d]. Compared to *B*, midtropospheric vertical velocity yielded similar results for deep convective clouds but was less successful in detecting low clouds (Figures S3 and S4).

The entire SST relative frequency distribution shifts almost uniformly to warmer SSTs with tropics-wide warming (Figure 2c), demonstrating that the observed “cliff” in the relative frequency distribution is not indicative of an upper limit on SST imposed by deep convection. Unlike SST, the relative frequency distribution of *B* is almost invariant between the warmest and coldest years (Figure 2d), implying that the area covered by deep convection does not substantially increase in response to tropics-wide warming. Approximate invariance of the *B*distribution was also seen in climate model projections [*Williams et al.*, 2009].

Results from the CAM5-AMIP simulation (Figures 2e–2h) also show a shift in the SST threshold for deep convection with tropics-wide warming (Figures 2e and 2g), and a collapse of the CRE distributions onto a single curve in *B* coordinates for the three warmest (1987, 1997, and 2003) and coldest (1984, 1985, and 1988) simulated years (Figure 2f). Modeled CRE is stronger than observed for deep convective regimes ($B > 0$) (Figures 2e and 2f), and modeled *B* (Figure 2h) is slightly higher than observed (Figure 2d), with a peak just above 0. However, the shift in SST threshold for deep convection is similar to that seen in global climate model simulations in response to CO_2 doubling [*Williams et al.*, 2009, Figures 1a and 1c] and indicates that the models are reliably capturing the response of convective threshold SST to tropics-wide warming.

A limitation of reanalysis-derived *B* is that it may be affected by the atmospheric model used in the reanalysis. We compared ECMWF to twice daily radiosonde profiles from the Atmospheric Radiation Measurement (ARM) site on Nauru Island (0.5°S, 166.9°E) using monthly temperature and relative humidity for years 1999–2012 [*Ciesielski et al.*, 2009]. Nauru is on the

eastern edge of the western Pacific warm pool and sees a reduction in cloudiness (corresponding to negative *B*) during La Niña [*Long et al.*, 2013]. Variations in the ARM-derived *B* closely tracked the ECMWF-derived *B* (Figure S5).

4 Inferred Cloud Feedbacks in Deep Convective and Stable Regimes

We estimated short-term cloud radiative feedbacks by regressing monthly adjusted CRE anomalies (departures from monthly climatology) against surface temperature anomalies [*Gregory et al.*, 2004], using monthly tropical average surface air temperature [e.g., *Zelinka and Hartmann*, 2011]. These estimates, hereafter denoted by $\Delta CRE_{adj}/\Delta T$, were categorized into convective regimes by calculating the regression slopes conditional on *B*. Shortwave and longwave $\Delta CRE_{adj}/\Delta T$ were substantially larger for deep convective clouds ($B > 0$) than for stable clouds in both CERES observations (Figure 3a) and CAM5-AMIP (Figure 3b), consistent with previous studies (based on cloud top pressure (CTP)) that inferred large but nearly canceling shortwave (positive) and longwave (negative) cloud feedbacks from high clouds [*Zelinka and Hartmann*, 2011; *Zhou et al.*, 2013]. The positive shortwave $\Delta CRE_{adj}/\Delta T$ here is slightly less effective at canceling the negative longwave $\Delta CRE_{adj}/\Delta T$, resulting in a net negative $\Delta CRE_{adj}/\Delta T$from deep convection (Figure 3c). This is not necessarily inconsistent with the small positive high-cloud feedback inferred previously [*Zelinka and Hartmann*, 2011; *Zhou et al.*, 2013], given uncertainties in both estimates, and because not all high clouds occur in deep convective regimes. Estimates of $\Delta CRE_{adj}/\Delta T$ using ω_{500} instead of *B* were qualitatively similar but of smaller magnitude (Figure S6), suggesting that *B* better characterizes the diversity of cloud responses to warming.

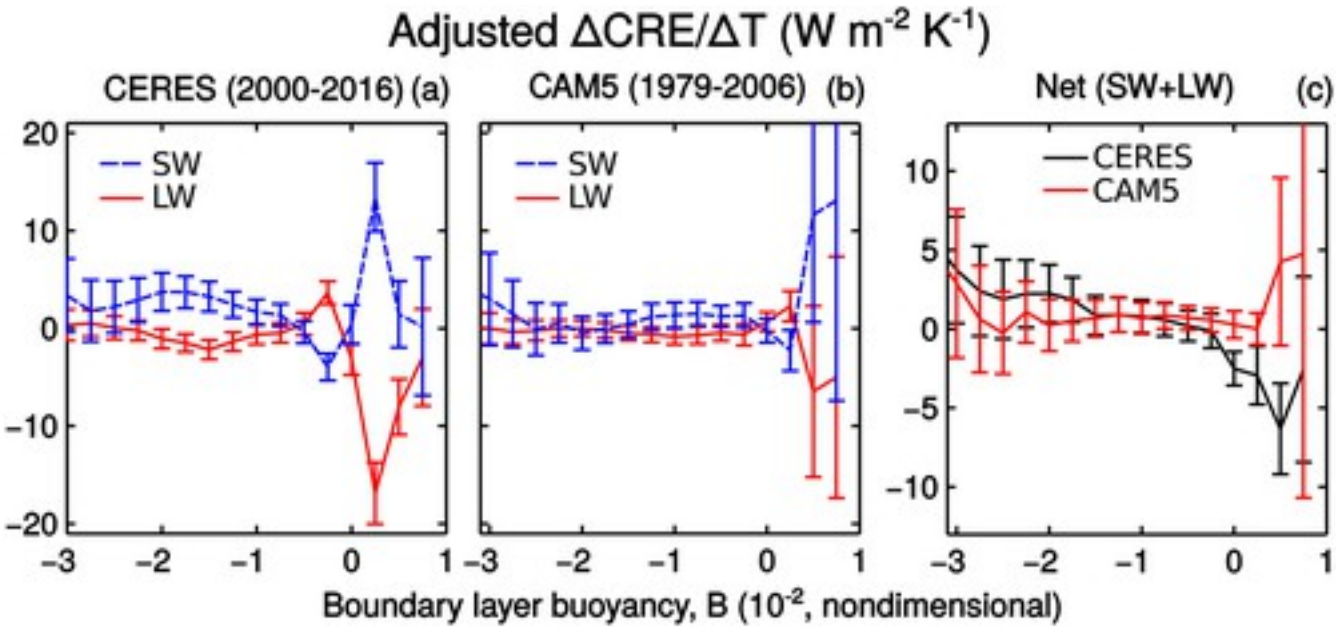

Figure 3

Open in figure viewerPowerPoint

Change in CRE per kelvin tropical warming ($\Delta CRE_{adj}/\Delta T$), estimated by linear regression of adjusted CRE against tropical average temperature anomalies within each 0.25×10^{-2} buoyancy interval. (a) Observed (CERES) shortwave (SW; dashed blue) and longwave (LW; red) $\Delta CRE_{adj}/\Delta T$are large in magnitude but of opposite sign in the deep convective regime ($B > 0$). (b) Shortwave and longwave $\Delta CRE_{adj}/\Delta T$ in CAM5 are smaller in magnitude than observed. (c) The net $\Delta CRE_{adj}/\Delta T$ from deep convection is positive in CAM5 (red) but negative in CERES (black), while the net $\Delta CRE_{adj}/\Delta T$ from stable cloud regimes ($B < 0$) is less positive in CAM5 than in CERES. Error bars indicate the 95% confidence interval for regression slope.

Caption

Relative to the observational estimate, CAM5-AMIP underestimated the negative longwave $\Delta CRE_{adj}/\Delta T$ from deep convection (Figure 3b) and underestimated the positive shortwave $\Delta CRE_{adj}/\Delta T$ from stable regimes. This result did not change by restricting the comparison to years 2000–2006 for which CAM5-AMIP and CERES observations were both available, although the shorter period increased the uncertainty (not shown). A similar result suggesting a positive cloud feedback in stable regimes can be seen in Figure 2b, in terms of a reduction in (negative) shortwave CRE during the 2015–2016 El Niño, particularly for B between −3 and −0.5 ($\times 10^{-2}$). Most of the discrepancy at $B = 0.5$ is due to the observed longwave response being more negative, despite the model's shortwave CRE having larger mean state biases for $B > 0$ (cf. Figures 2b and 2f). This implies that mean state biases as a function of B are not trivially related to the biases in the response to warming. Note that the larger error bars for CAM5-AMIP in Figure 3b are due to larger scatter about the linear fit.

We estimated contributions of convective regimes to the net $\Delta CRE_{adj}/\Delta T$ (supporting information Table S1) by multiplying $\Delta CRE_{adj}/\Delta T$ in Figure 3 by the relative frequency of *B* bins. Feedbacks from stable and deep convective clouds were nearly equal and of opposite sign, contributing to a smaller net feedback in the observations (-0.06 ± 0.73 $Wm^{-2}K^{-1}$). The degree of this cancelation and the negative sign of the net $\Delta CRE_{adj}/\Delta T$ from deep convection was not captured in CAM5. This biased response may be related to the higher climate sensitivity seen in some models [*Mauritsen and Stevens*, 2015]. However, CAM5 also underestimated the positive $\Delta CRE_{adj}/\Delta T$ from stable regimes, such that the net $\Delta CRE_{adj}/\Delta T$ summed across all regimes (0.35 ± 0.65 $Wm^{-2}K^{-1}$) was within statistical uncertainty of the observations. The per Kelvin change in the probability of *B* regimes (Figure S7) was relatively small, contributing -0.15 $Wm^{-2}K^{-1}$ and -0.01 $Wm^{-2}K^{-1}$ to the observed and modeled $\Delta CRE_{adj}/\Delta T$, respectively. For tropical ocean and land together, we inferred net short-term cloud feedbacks of -0.51 ± 0.58 $Wm^{-2}K^{-1}$ in observations, and -0.60 ± 0.45 $Wm^{-2}K^{-1}$ in CAM5-AMIP, similar to previous estimates [*Trenberth et al.*, 2010].

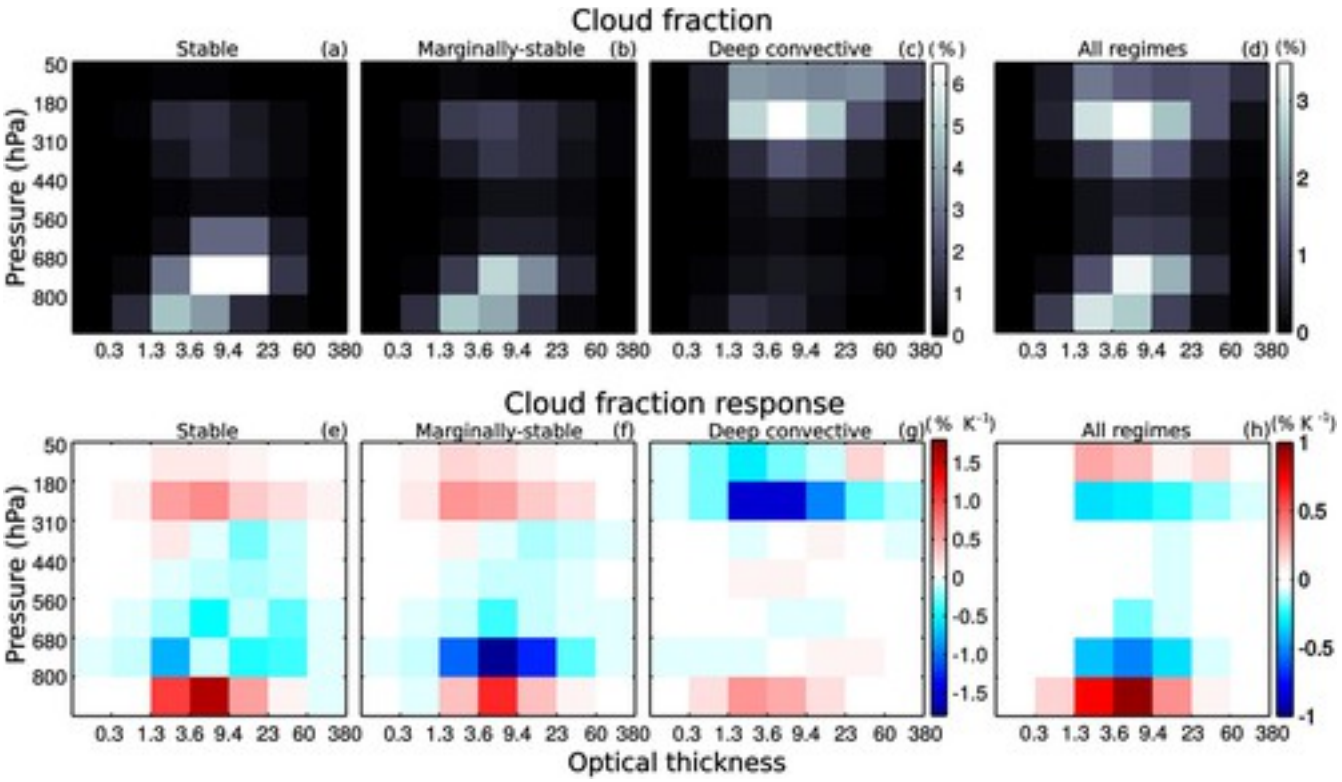

Figure 4

Open in figure viewerPowerPoint

MODIS cloud fraction (%) separated into cloud top pressure and optical thickness bins for (a) stable ($-3 < B\times10^2 < -2$), (b) marginally stable ($-2 < B\times10^2 < 0$), (c) deep convective ($0 < B\times10^2 < 1$), and (d) all regimes. (e–h) As in Figures 4a–4d but for the cloud fraction response to

warming estimated by the slope of the linear regression of cloud fraction anomalies against tropical average temperature anomalies.
Caption

Since stable regimes are not guaranteed to be free of high clouds, we used MODIS (Moderate Resolution Imaging Spectroradiometer) Collection 5 data to identify clouds by CTP and optical thickness (Figures 4a–4d) [*King et al.*, 2003; *Pincus et al.*, 2012]. The results confirm that some high clouds (CTP < 440 hPa) occur in stable regimes, while most high clouds and almost all optically thick high clouds occur in deep convective regimes diagnosed by $B > 0$. It is noted that these histograms may change with the more reliable Aqua MODIS Collection 6 [*Yue et al.*, 2016].

We estimated the cloud response to warming (Figures 4e–4h) using the slope of the linear regression of cloud fraction anomalies against tropical average temperature anomalies [e.g., *Zelinka and Hartmann*, 2011]. High-cloud fraction declined with warming in deep convective regimes ($-6.4 \pm 2.8\%K^{-1}$) but increased in stable and marginally stable regimes ($1.1 \pm 1.2\%K^{-1}$). Given their opposite sign, these differences are unlikely to be explained by differences between local and tropical average warming. Warming occurred in all regimes, although the deep convective regime warmed more (Figure S8). Furthermore, there is a distinct upward shift in high-cloud fraction in the $B < 0$ regimes, but not in the $B > 0$ regimes. High-cloud CTP decreased by 31 ± 20 hPa K^{-1} in stable regimes but did not significantly change (0 ± 24 hPa K^{-1}) in deep convective regimes, as estimated by regression of CTP anomalies against tropical average surface temperature anomalies. This indicates that different processes govern temperature responses of high clouds in deep convective regimes compared to those that occur remotely from deep convection. The latter may be formed in situ or may be advected into stable regimes from deep convective regimes.

The compensating changes in high-cloud fraction between stable and deep convective regimes resulted in smaller net changes in high clouds with warming (Figure 4h), that are consistent with previous studies [*Zelinka and Hartmann*, 2011; *Zhou et al.*, 2013]. The reduction in deep convective high-cloud fraction is consistent with the inferred negative longwave cloud feedback in deep convective regimes (Figure 3a). Note that cloud responses in stable regimes were not statistically significant, in part due to compensating responses in different regions (Figure S1). It is also noted that feedbacks inferred from tropical interannual variability are not necessarily indicative of global feedbacks [*Trenberth et al.*, 2010], and short-term cloud feedbacks may differ from long-term global warming cloud feedbacks [*Zelinka and Hartmann*, 2011; *Zhou et al.*, 2015, 2016]. The B coordinate may provide some remedy for the timescale dependence of

cloud feedbacks, by attempting to control for short-term variations in the large-scale circulation and its coupling to convective instability.

5 Conclusions

The observations confirm two predictions of climate models: As a function of subcloud buoyancy (B), the threshold for deep convection is nearly invariant with tropics-wide warming, such that cloud radiative effect (CRE) during the warmest and coldest years tends to collapse onto a single curve in B coordinates. Second, the frequency distribution of B is approximately invariant with warming, thus constraining the relative frequency of deep convective regimes. Applying this diagnostic to short-term observations, we inferred a negative cloud feedback in deep convective regimes that was not represented in CAM5. Our results suggest that high clouds respond differently to warming in deep convective compared to stable regimes. Compensation between these responses contributed to the small magnitude and uncertain sign of the observed net tropical cloud radiative feedback inferred from short-term changes in adjusted CRE. Understanding the different processes governing cloud feedbacks in stable and deep convective regimes will be important in refining climate model representation of cloud feedbacks.

Acknowledgments

The CERES EBAF-TOA Ed2.8 data set was obtained from the NASA Langley Research Center Atmospheric Science Data Center, at http://ceres.larc.nasa.gov. The ECMWF interim reanalysis data were obtained from ECMWF public data sets web interface at http://www.ecmwf.int/en/research/climate-reanalysis/era-interim. CAM5-AMIP data were obtained from https://www.earthsystemgrid.org/dataset/ucar.cgd.ccsm4.cam5.1.amip.1d.002.html. Nauru radiosonde data were obtained from https://doi.org/10.5439/1095390. MODIS data were obtained from CFMIP observations for model evaluation (http://climserv.ipsl.polytechnique.fr/cfmip-obs/) at ftp://laadsweb.nascom.nasa.gov/NetCDF/L3_Monthly/V02/. We thank Mark Zelinka and an anonymous reviewer for helpful comments and suggestions. This material is based upon work supported in part by the U.S. Department of Energy, Office of Science, Office of Biological and Environmental Research, under contract DE-AC02-05CH11231.